Accuracy of Sea Ice Floe Size Observation from an Aerial Camera at Slant Angles

Christopher Dahlin Rodin[1] and Tor Arne Johansen[2]

***Abstract*— The importance of measuring the size of ice floes in e.g. marine navigation and environmental sciences has made it a frequently performed procedure. When real-time data is required, images from a camera on-board an aerial vehicle or mounted on a marine vessel is commonly preferred over satellite images. Their lower fields of view can be improved by tilting the cameras to capture images of a larger area. However, this introduces a greatly changing ground resolution within the same camera image, which makes size estimation a more complex task. It is nevertheless performed in several methods to estimate the size of ice floes. In this paper, ice floe size estimation is evaluated for different scenarios when using an aerial camera at slant angles. In order to reduce errors caused by automatic image segmentation and attitude estimation algorithms, the methods are aided by human input. The estimates are performed on real world data captured during the Statoil Station Keeping Trials in the Bothnian Bay during March 2017. The results conclude that the major challenge is to guarantee separation between ice floes in the camera images, which is something that requires both enough ground resolution and a suitable image segmentation algorithm.**

I. Introduction

Sea ice occupies approximately 7% of the surface area of the world oceans [1], and comes in different shapes such as icebergs, which have been broken off from a glacier or an ice shelf, and ice floes, which are pieces of sea ice varying in size from a few meters to tens of kilometers across [2]. Sea ice has a major effect on weather, climate, and ocean currents [3], and can also significantly obstruct navigation in places such as the Northern Sea Route [4]. Both smaller and larger ice formations undergo large changes throughout a year [5]. This makes continuously monitoring sea ice a vital part in a number of fields.

There exist a number of methods for monitoring ice floes. Haugen et al. [6] provides an overview of existing sensors and sensor platforms for ice management. Using a satellite as a sensor platform allows for very high quality sensors and a large field of view from cameras and radars carried by the satellite. However, due to their high altitude, the spatial resolution is limited. Satellite images can also be costly, and the updates are slow. Additionally, some sensors carried by satellites can not properly sample the ground environment during certain weather conditions such as clouds. An alternative to a satellite is a high-altitude aircraft. An aircraft can carry many of the same sensors as a satellite while operating at a lower altitude, which allows for higher spatial and temporal resolution than the satellite. Using a high-altitude aircraft as a sensor platform is however expensive, in particular in remote areas such as the Arctic or when continuous updates of the environment are required. If the goal is to obtain sea ice data around a marine vessel, a solution is to attach the sensors to the vessel itself. An example of this is marine radars used for navigation and collision avoidance. The data from the sensors come in real-time, and have a high spatial resolution for areas near the vessel. However, the area covered by shipborne sensors is often small. A similar scenario is when the sensors are placed on land, which has similar benefits and limitations.

In between the high-altitude airborne sensors and the shipborne sensors are the recent emergence of Unmanned Aerial Vehicles (UAVs) as a sensor platform when gathering ice data – in particular UAVs small enough to take off from and land on a marine vessel [6] [7]. These UAVs often operate at a lower altitude, allowing for real-time data at a high spatial resolution, even though the weight of the sensors are limited. The sensors carried by UAVs can cover a higher area than those carried by the marine vessel, but not quite as big as a satellite or a high-altitude aircraft. A similar sensor platform is an aerostat moored to a marine vessel. The aerostat can not move around like a UAV in order to cover a larger area, but it benefits from a higher altitude than the sensors attached to a marine vessel and requires little supervision. A camera mounted to an aerostat or a small UAV is therefore suitable when monitoring sea ice in an area near a vessel, but the spatial coverage of shipborne sensors are not enough.

In order to be able to increase the field of view further of a camera attached to a marine vessel, a UAV, or an aerostat, the camera can be tilted. If the tilt angle and other camera parameters are known, the pinhole camera model [8] can be used to find the world coordinates of a pixel in the camera image. Several methods use this to rectify camera images and measure the size of ice floes [9] [10]. Since the

The authors would like to thank Statoil, Viking Ice Consultancy and Viking Supply Ships for contributing to a safe Station Keeping Trials in Ice in 2017. Statoil is acknowledged for supporting this research. This project has received funding from the European Unions Horizon 2020 research and innovation programme under the Marie Skłodowska-Curie grant agreement No 642153. The information presented in this paper reflects only the authors view, and the Agency is not responsible for any use that may be made of the information it contains. The work was also supported by the Research Council of Norway through the Centre for Autonomous Marine Operations and Systems (NTNU-AMOS).

[1]Christopher Dahlin Rodin is with Center for Autonomous Marine Operations and Systems, Department of Engineering Cybernetics, Norwegian University of Science and Technology, Trondheim, Norway and Maritime Robotics, Trondheim, Norway christopher.rodin@ntnu.no

[2]Tor Arne Johansen is with Center for Autonomous Marine Operations and Systems, Department of Engineering Cybernetics, Norwegian University of Science and Technology, Trondheim, Norway tor.arne.johansen@ntnu.no

image capturing process is complex, in particular with greatly varying distances in an outdoor environment such as that of a tilted camera measuring ice floe sizes, it is of interest to evaluate how well it is possible to estimate the ice floe size when the camera is tilted at slant angles.

A method developed by Lu & Li [10] for obtaining the size of ice floes from camera images when the camera is tilted was evaluated by the same authors against a more direct method, by comparing the ice floe distributions calculated by both methods. However, the authors only evaluates their simplified method, and not the effects of having a camera at a slant angle. A qualitative evaluation of size estimation for different camera-to-object angles (see Appendix I for the definition of camera-to-object angle) could provide guidelines for when a good ice floe size estimate can be expected.

In this paper, a method for estimating the dimensions of individual ice floes is presented. The main goal of the method is to be used in evaluating the size estimation of individual ice floes seen at different camera-to-object angles. Manual methods with high accuracy are therefore preferred over automatic methods, in order to reduce errors caused by e.g. image segmentation errors. The method is applied to experimental data from the Statoil Station Keeping Trials performed in the Bothnian Bay during the first three weeks of March 2017. The results are evaluated and discussed in order to find how well the size of ice floes can be estimated for different scenarios when a large camera-to-object angle is used.

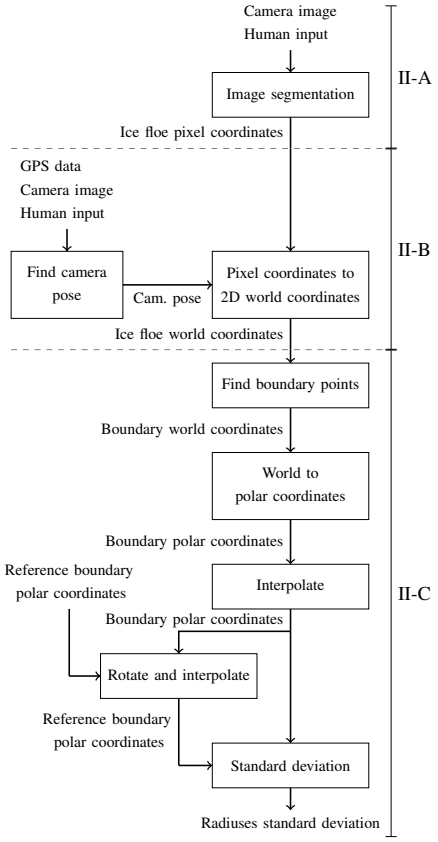

Fig. 1. Overview of the size estimation and evaluation algorithm. The rightmost text indicates which section contain that details about each part.

II. Methodology

This section contains explanations of the methods used in this paper for comparing the dimension estimates of an ice floe appearing in multiple camera images at different camera-to-object angles. Figure 1 shows an overview of the methods. Lastly, the size estimation error that can be explained by a difference in ground resolution is explained.

A. Finding the pixels representing an ice floe

In order to find the pixels representing an ice floe in a camera image, the image is first segmented. Segmentation divides an image into regions or objects [11]. In this case, the ice floes are separated from other objects such as water, brash ice, and other ice floes. Errors made by the image segmentation algorithm, such as dividing one ice floe into two segments, or missing a border between two ice floes labelling them as the same segment, can have a big impact on the size estimate.

Even though image segmentation methods have existed for a long time, humans still outperform commonly available algorithms [12]. Recent algorithms have started to outperform humans [13], but human performance in image segmentation is still often used as the ground truth when evaluating algorithms. In this paper, human image segmentation aided by flood-fill algorithm is used to find the pixels representing an ice floe in an image due to its simplicity.

The flood-fill algorithm selects connected pixels with an intensity within a certain threshold from that of the starting pixel [14], and is run after the image has been converted to gray-scale. After the flood-fill algorithm has been run, a human adjusts the segmentation by manually adding or removing regions of pixels to properly represent the area occupied by the ice floe in the camera image.

B. Image to world coordinates

The pinhole camera model [8] is used to model the projection of world coordinates onto an image plane. The projection is given by

$$\lambda \begin{bmatrix} x_i \\ y_i \\ 1 \end{bmatrix} = \Lambda \begin{bmatrix} \Omega & \tau \end{bmatrix} \begin{bmatrix} x_w \\ y_w \\ z_w \\ 1 \end{bmatrix} \tag{1}$$

where x_i, y_i, and $p_w = [x_w \; y_w \; z_w]^T$ are the pixel coordinates and world coordinates of the projected point respectively, λ is a scaling factor, Λ is the intrinsic camera matrix obtained by camera calibration, and Ω and τ are the rotation matrix and translation vector from world coordinates to camera coordinates respectively.

The world coordinate system is in this case defined as the local tangent plane of the Earth at the location of the camera at sea level, with the x-axis pointing east, the y-axis pointing down, and the z-axis pointing north. By solving (1) for x_w

and z_w, it is possible to obtain the world coordinates of a point if its pixel coordinates and world coordinate y_w are known. The change in y_w due to the curvature of the Earth and the altitude of the ice floes are disregarded, and y_w is thus set to zero.

The pinhole camera model assumes that the rotation matrix and translation vector from world coordinates to camera coordinates are known. In this paper the exact world position of a point represented by a pixel in the camera image is not required, but rather the distance from the camera to the point. Rotating the camera around its y-axis (yaw) or moving the camera in the xz-plane will not change this calculated distance. This means that there is only a need to estimate the negative camera altitude, τ_y, and the camera rotations around its x- and z-axis (pitch and roll).

The camera altitude is estimated using a GPS unit. The roll and pitch are estimated by projecting horizon points onto the camera image using (1), and then manually adjusting the roll and pitch until the horizon points match the horizon in the camera image. The method for finding the world position of horizon points is described in Appendix II. See figure 2 for an example of matching horizon points.

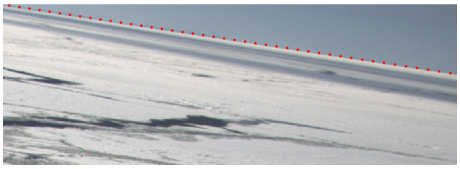

Fig. 2. The horizon points (red dots) matched with the horizon in a camera image.

C. Comparing ice floe size estimates

The aim of this paper is to evaluate the accuracy of the size estimates of an ice floe for different camera-to-object angles. The evaluation is done by comparing the size estimate of an ice floe with its reference. The reference is the size estimate of the same ice floe at the lowest camera-to-object angle available in the camera image set, i.e. it is the estimate least prone to errors. In order to make a quantitative evaluation of the results easier, a single metric of the accuracy will be used. It is possible to use e.g. the volume, but this can be misleading since vastly different shapes can result in the same volume. Instead, the standard deviation of the radiuses of an ice floe in polar coordinates from the reference is calculated as the error metric, σ_{radiuses}. This guarantees a larger error when the deviation from the reference is larger overall, and can be used in e.g. statistical simulations.

The standard deviation σ_{radiuses} will be evaluated against the camera-to-object angle, $\alpha_{\text{c-o}}$, for each ice floe. This is calculated as the mean camera-to-object angle for each x_w and z_w coordinate of the points representing the ice floe in the camera image.

After the x_w and z_w coordinates of the points representing the ice floe in the camera image have been obtained according to section II-A and II-B, they are mean centered.

An alpha shape [15] is then generated for the points in order to find a natural border of the ice floe. An alpha shape is a shape that encloses a set of points by defining the boundary points as those which can be touched by empty circles (i.e. circle not containing any points) with radiuses α. See figure 3 for a visual description of the alpha shape algorithm. The alpha shape boundary points are selected as

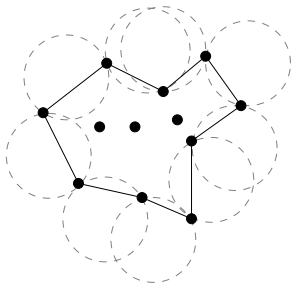

Fig. 3. The alpha shape algorithm visualized. The filled points represent the points, the grey dashed circles represent the empty circles connected to two points each, and the lines indicate which boundary points the alpha shape goes through.

the boundary points of the ice floe. The ice floe boundary points are transformed from Cartesian to polar coordinates according to

$$\begin{aligned} r_b &= \sqrt{x_w^2 + z_w^2} \\ \alpha_b &= \arctan\left(\frac{x_w}{y_w}\right) \end{aligned} \tag{2}$$

where r_b is the radius and α_b is the polar angle.

Since the ice floe will be rotated relative to the camera between camera images, and the resolution of the polar angle will change, the calculated radiuses of an ice floe in one camera image can not be directly compared with the radiuses of the ice floe in another image. In order to make them comparable, radiuses for predefined equidistant polar angles are found using piecewise cubic Hermite interpolation [16]. After the interpolation, the polar angles of the reference ice floe are shifted in order to find the polar angles which produces the lowest standard deviation σ_{radiuses}. This is equivalent to rotating one ice floe to match the other ice floe.

D. Ground Resolution Error

The ground resolution is the number of pixels per square meter when projected onto the sea surface. In order to find what accuracy is possible, the error that can be explained by the decrease in ground resolution as the camera moves away from the object – the ground resolution error, $\sigma_{\text{radiuses gr}}$ – is calculated for each ice floe in each camera image. This is done by shifting the mean of the world points of the reference to the mean of the ice floe being evaluated; projecting it onto the image coordinate system using (1); rounding the image coordinates to their closest integer values to simulate the precision lost; and then calculating the standard deviation σ_{radiuses} using the same methods as for the ice floe being evaluated.

The ground resolution error is not the theoretical minimum error for the given camera-to-object angle and ground

resolution. Rather, it is the approximation of how large part of the error that can be attributed to the ground resolution for the current image.

III. Experimental Setup

Experiments were performed in order to evaluate the accuracy of size estimates of ice floes using a camera at slant angles using the method described in section II. The experiments took place during the Statoil Station Keeping Trials (SKT) in the Bothnian Bay during the first three weeks of March 2017. The SKT involved two vessels in operation, Magne Viking and Tor Viking.

The camera system was mounted on the moored balloon system OceanEye made by Maritime Robotics, which in turn was attached to Magne Viking. The OceanEye allowed for the camera to stay at an altitude of around 120 meters throughout the day.

A. Camera System

The camera system consisted of an EO-camera, a lens, a GPS unit, and an on-board computer. The system was designed to capture images with low distortion, high time synchronization accuracy, and to be light weight. The details of the camera unit and lens can be found in table I.

TABLE I
Specification of the camera system

Camera	FLIR CM3-U3-31S4C-CS
Resolution	2048 x 1536 px
Pixel size	3.45 µm
Lens	Kowa LM8JC10M
Focal length	8.5 mm
Lens distortion	0.31 %

B. Scenarios

The camera was capturing images at 1 Hz for about eight hours per day. Since the process of estimating the dimensions of an ice floe in a camera image consists partly of manual work, the evaluation was limited to a camera image sequence of ten images, taken eight seconds apart. The sequence was chosen to be when Magne Viking was moving, in order to capture the same ice floes in multiple camera images at different camera-to-object angles. In the image sequence, five ice floes of different sizes were chosen. See figure 4 for a cropped camera image containing the five ice floes.

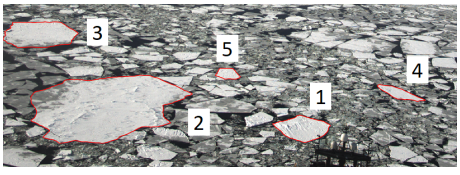

Fig. 4. A cropped camera image containing the five ice floes being analyzed.

IV. Results and Discussion

This section presents and discusses the experimental results together with the calculated theoretical errors. First, each step of the methods in section II is shown, followed by an analysis of the error metric, σ_{radiuses}.

The pixels are first selected using a flood-fill algorithm, and then adjusted by manually adding and removing pixel regions. See figure 5 for an example of this process.

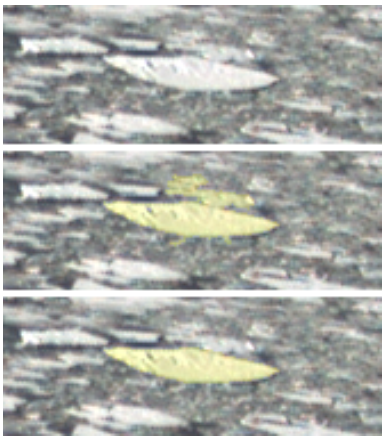

Fig. 5. The pixel selection process. The top image shows the raw camera image. The center image shows the pixels selected by the flood-fill algorithm in yellow. The bottom image shows the final results after after manually adjusting the pixels selected by the flood-fill algorithm.

After the ice floe pixels have been selected, their corresponding position in the world coordinate system are found, assuming an ice floe altitude of zero. The mean is subtracted from the points in both dimensions, x_w and y_w, and an alpha shape around the points is calculated. See figure 6 for the mean-centered points in the world coordinates, together with the alpha shape.

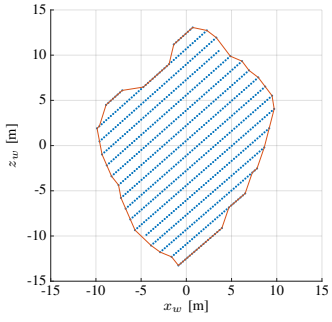

Fig. 6. The corresponding mean centered world coordinates of the selected pixels (blue dots) and the alpha shape (red curve).

The points connected to the border of the alpha shape are then transformed into polar coordinates, and interpolated using piecewise cubic Hermite interpolation for polar angles in the interval $[0°, 360°)$, with a resolution of $1°$. See figure 7 for the interpolated border points in polar coordinates.

The same methods were applied to the ice floe in the reference camera image. The ice floe reference was then

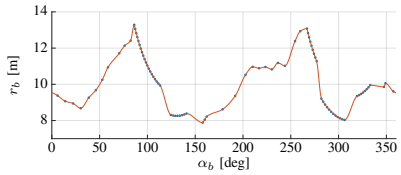

Fig. 7. The border points in polar coordinates (blue dots), and a curve going through the interpolated points (red line).

rotated to match the current points of the ice floe being evaluated. See figure 8 for a comparison of the ice floe points being evaluated in Cartesian coordinates, the reference points of the ice floe, and the rotated reference points.

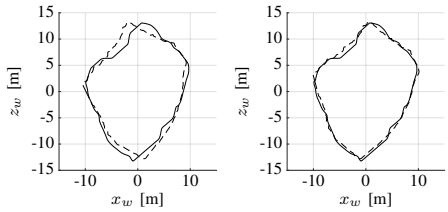

Fig. 8. The ice floe in the camera image being evaluated versus in the reference image without any rotation (left). The ice floe in the camera image being evaluated versus in the reference image rotated to match the first (right).

The distance and camera-to-object angle to the ice floe being evaluated is in this case 623 m and 81.4° respectively, and 262 m and 70.1° respectively for the reference. The standard deviation σ_{radiuses} is 0.40 m, and $\sigma_{\text{radiuses gr}}$ is 0.33 m.

The same algorithm is then applied to the five ice floes in the selected camera image set. See figure 4 for the numbered ice floes in the camera image with the smallest camera-to-object angle. The resulting error metric σ_{radiuses} and ground resolution error metric $\sigma_{\text{radiuses gr}}$ are then presented in figure 9. The ice floe number in the top left corner of each graph corresponds to the ice floe numbers in figure 4.

The errors generally increase with an increased camera-to-object angle, as was expected. There is little to be discussed for ice floe 1 – the error generally increases with an increased camera-to-object angle, and stays slightly above the ground resolution error. The difference between the error and the ground resolution error might be explained by inconsistency in the pixel selection process and remaining errors from the camera calibration. The error for ice floe 4 sometimes dips below the ground resolution error. This might happen when the ice floe in the camera images line up well with the pixel edges, or when an error has occurred when selecting the ice floe pixels in the reference image.

The error for ice floe 5 makes a sudden jump between $\alpha_{\text{c-o}}$ 76.5° and 77.8°, and a similar phenomena can be seen for ice floe 3 between 82° and 82.5°. By analyzing the camera images, it can be seen that this is because the border between nearby ice floes can no longer be seen, making them appear as one ice floe. See figure 10 for a comparison between the reference image and the fourth image (camera-to-object angle of 78.8°) of ice floe 5, where the loss of separation between the ice floe and a nearby ice floe can be seen.

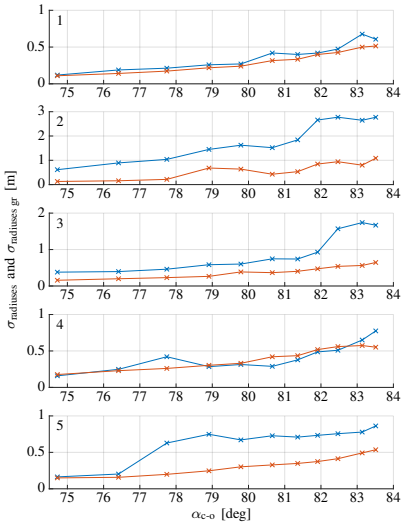

Fig. 9. The resulting standard deviations σ_{radiuses} (blue line) and $\sigma_{\text{radiuses gr}}$ (red line) versus the camera-to-object angle. The number in the top left corner of each graph indicates which ice floe is being evaluated, see figure 4.

Fig. 10. Ice floe 5 in the reference camera image (left) and with a camera-to-object angle of 77.8° (right).

The large error produced by diminishing borders indicate that the separation between ice floes are of high importance when estimating the size of ice floes.

The errors for ice floe 2 and 3 are overall quite large. Looking at figure 4, it can be seen that these ice floes are larger than the others, both contain darker areas, and both are near brash ice. This pose a problem to both the flood-fill algorithm and to human segmentation since it is more difficult to manually correct minor errors for large ice floes, and ice floes with poorly defined borders.

V. Conclusion

In this paper, a method for estimating the size of individual ice floes has been presented, as well as a metric to evaluate the accuracy of the size estimation. The method, which was designed to minimize the errors caused by automatic image segmentation and attitude estimation algorithms in order to find the limitations of the camera system when estimating the size of ice floes at slant angles, is applied to experimental data collected during the Statoil SKT performed in the Bothnian Bay in March 2017. During the experiment, the camera was moved in relation to the ice floes in order to capture camera images of the same ice floes at different distances, which allowed for the evaluation of ice floe size

estimation for different camera-to-object angles. Evaluation of the resulting errors and the camera images conclude that the size of an ice floe can be estimated with a high accuracy if some criteria, which allows for the ice floes to be accurately segmented in the camera images, are met. This makes it important to take into account not only the size estimation accuracy of an individual ice floe when designing a camera system for a certain ground resolution, but also the separation between ice floes.

Potential future work includes an evaluation of more automatic image segmentation and size estimation algorithms for use when estimating the size of ice floes. The camera images could also be fused with e.g. Synthetic Aperture Radar (SAR) images in order to find details not visible in camera images. The geometrical calculations can also be made more rigorous by e.g. taking into account the effect of ice ridges on the ice floes, which might affect the results at a large camera-to-object angle.

APPENDIX I
CAMERA-TO-OBJECT ANGLE

The camera-to-object angle, α_{c-o}, is defined as the angle between a vector pointing straight down from the camera, $\mathbf{a}_{\text{c-g}}$, and a vector pointing from the camera towards the object, $\mathbf{a}_{\text{c-o}}$. See figure 11 for a visual description.

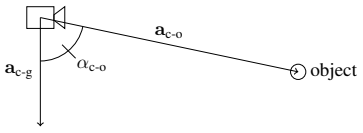

Fig. 11. The camera-to-object angle, $\alpha_{\text{c-o}}$.

The camera-to-object angle can be calculated according to

$$\alpha_{\text{c-o}} = \cos^{-1}\left(\frac{\mathbf{a}_{\text{c-g}} \cdot \mathbf{a}_{\text{c-o}}}{||\mathbf{a}_{\text{c-g}}||\ ||\mathbf{a}_{\text{c-o}}||}\right) \tag{3}$$

APPENDIX II
HORIZON POINTS

The first step in finding a horizon point is to find the angle between the camera and the horizon, γ, which is given by

$$\gamma = \cos^{-1}\left(R/(R+a)\right) \tag{4}$$

where R is the radius of the Earth, and a is the camera altitude. See figure 12 for the geometrical derivation of (4). Note that this approximates the oblate spheroid shape of the Earth with a spherical shape.

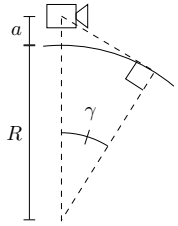

Fig. 12. The geometric derivation of the angle between the camera and the horizon, γ.

When the angle γ has been acquired, the y_w and z_w position of the horizon, $y_{w\text{ horizon}}$ and $z_{w\text{ horizon}}$, can be acquired according to

$$\begin{aligned} y_{w\text{ horizon}} &= R(1-\cos\gamma) \\ z_{w\text{ horizon}} &= R\sin\gamma \end{aligned} \tag{5}$$

See figure 13 for the geometrical derivation of (5). The x_w-coordinate of the horizon point, $x_{w\text{ horizon}}$, is simply set to zero. $x_{w\text{ horizon}}$ and $z_{w\text{ horizon}}$ are then rotated around the y-axis with equidistant angles in order to obtain the world coordinates of several horizon points.

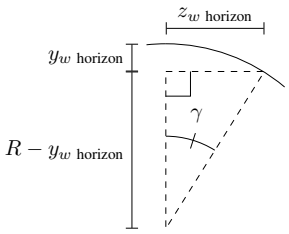

Fig. 13. The geometric derivation of the y_w and z_w position of the horizon.

REFERENCES

[1] P. Wadhams, *Ice in the Ocean*. Taylor & Francis, New York, 2000.

[2] J. Bischof, *Ice drift, ocean circulation and climate change*. Springer, 2000.

[3] M. Shokr and N. Sinha, *Sea Ice: Physics and Remote Sensing*, ser. Geophysical Monograph Series. Wiley, 2015.

[4] O. Johannessen, V. Alexandrov, I. Frolov, S. Sandven, L. Pettersson, L. Bobylev, K. Kloster, V. Smirnov, Y. Mironov, and N. Babich, *Remote Sensing of Sea Ice in the Northern Sea Route: Studies and Applications*, ser. Springer Praxis Books. Springer Berlin Heidelberg, 2006.

[5] D. K. Perovich and K. F. Jones, "The seasonal evolution of sea ice floe size distribution," *Journal of Geophysical Research: Oceans*, vol. 119, no. 12, pp. 8767–8777, 2014.

[6] J. Haugen, L. Imsland, S. Løset, R. Skjetne *et al.*, "Ice observer system for ice management operations," in *Proc. International Offshore and Polar Engineering Conference*, Maui, Hawaii, USA, 2011.

[7] F. S. Leira, T. A. Johansen, and T. I. Fossen, "A uav ice tracking framework for autonomous sea ice management," in *Proc. IEEE International Conference on Unmanned Aircraft Systems (ICUAS'17)*, Miami, Florida, USA, 2017.

[8] S. J. D. Prince, *Computer Vision: Models, Learning, and Inference*, 1st ed. New York, NY, USA: Cambridge University Press, 2012.

[9] Q. Zhang and R. Skjetne, "Image processing for identification of sea-ice floes and the floe size distributions," *IEEE Transactions on Geoscience and Remote Sensing*, vol. 53, no. 5, pp. 2913–2924, May 2015.

[10] P. Lu and Z. Li, "A method of obtaining ice concentration and floe size from shipboard oblique sea ice images," *IEEE Transactions on Geoscience and Remote Sensing*, vol. 48, no. 7, pp. 2771–2780, July 2010.

[11] R. Gonzalez and R. Woods, *Digital Image Processing*. Pearson/Prentice Hall, 2008.

[12] R. Vidal, Y. Ma, and S. Sastry, *Generalized Principal Component Analysis*, ser. Interdisciplinary Applied Mathematics. Springer New York, 2016.

[13] Y. Guo, Y. Liu, A. Oerlemans, S. Lao, S. Wu, and M. S. Lew, "Deep learning for visual understanding: A review," *Neurocomputing*, vol. 187, pp. 27 – 48, 2016.

[14] W. Burger and M. Burge, *Digital Image Processing: An Algorithmic Introduction Using Java*. Springer London, 2016.

[15] H. Edelsbrunner, D. Kirkpatrick, and R. Seidel, "On the shape of a set of points in the plane," *IEEE Transactions on information theory*, vol. 29, no. 4, pp. 551–559, 1983.

[16] C. de Boor, *A Practical Guide to Splines*. Springer-Verlag New York, 1978.